JOURNAL OF SOLID STATE CHEMISTRY **138,** 193–200 (1998)
ARTICLE NO. SC987771

Structural Modifications and Electrochemical Behavior of Lithium-Inserted $In_{16}Fe_8S_{32}$

C. Pérez Vicente, C. Bousquet, A. Krämer, J. L. Tirado,* J. Olivier-Fourcade, and J. C. Jumas[1]

*Laboratoire de Physicochimie de la Matière Condensée (UMR 5617 CNRS), Université de Montpellier II, Place Eugène Bataillon, 34095 Montpellier Cedex 5, France; and *Laboratorio de Química Inorgánica, Facultad de Ciencias, Universidad de Córdoba, Avenida San Alberto Magno s/n, 14004 Córdoba, Spain*

Received September 24, 1997; in revised form January 27, 1998; accepted February 3, 1998

We have studied the structural modifications that occur during electrochemical insertion of lithium into the spinel compound $In_{16}Fe_8S_{32}$. Studies by X-ray diffraction (Rietveld analysis) and Mössbauer spectroscopy of the lithiated products indicate that some cation migration takes place during the insertion process. The Mössbauer spectra show that no reduction of Fe^{2+} takes place during the insertion. The variation of the isomer shift indicates an increase in the covalency of the network. The results of the X-ray absorption experiments show the absence of a clear reduction of In^{3+} and the incorporation of incoming electrons into the delocalized band structure. Analysis of the discharge curve shows the presence of two different domains. For the first one there is a small interaction between inserted ions. The second one shows a repulsive interaction and a decrease in the diffusion coefficient.

INTRODUCTION

The spinel structure compounds provide suitable host lattices for the insertion of electron donor elements because of the presence of many vacant sites. The different oxidation states of the metallic elements that may be present in these solids make favorable the electron transfer process taking place during the redox insertion reactions. Thus, several interesting candidates for applications as electrode in lithium and rocking-chair batteries have been found among solids with spinel-related structure (1–6).

The structural formula of an idealized spinel phase is commonly written $(A)_{Td}[B_2]_{Oh}X_4$. It consists of a close-packed array of X anions with one-eighth of the tetrahedral interstices (Td) and one-half of the octahedral ones (Oh) filled by cations. In a normal spinel, A cations are placed in Td sites, whereas in a completely inverse spinel, these sites are filled by B cations exclusively (7). Several indium compounds, such as high-temperature indium sesquisulfide, ternary sulfides MIn_5S_8, (M = Cu, Ag) and MIn_2S_4, (M = Mn, Fe, Co, Ni), and cation-deficient $SnIn_4S_8$, are some examples of indium-based spinel sulfide compounds (4, 5).

Recently (8), we reported the insertion properties of chemically lithiated $In_{16}Fe_8S_{32}$, characterized by X-ray diffraction and Mössbauer spectroscopy. Iron-substituted indium spinel compound offers additional opportunities for a detailed study of the insertion process by ^{57}Fe Mössbauer spectroscopy. This technique allows us to obtain information about the local environment of iron atoms in the structure.

In this paper, we report a fundamental study on the structural modifications that occur during electrochemical lithium insertion in the spinel compound $In_{16}Fe_8S_{32}$. This structural characterization is carried out by X-ray diffraction (Rietveld analysis), ^{57}Fe Mössbauer spectroscopy, and X-ray absorption spectroscopy at L_I edge of In. Additional information comes from analysis of the discharge curves and diffusion coefficient data.

EXPERIMENTAL

A powdered sample of $In_{16}Fe_8S_{32}$ was prepared as described elsewhere (8). Electrochemical lithium insertion was carried out at room temperature in two-electrode test cells using the indium, iron thiospinel as cathode, lithium metal foil as anode, and 1 M solution of $LiClO_4$ in propylene carbonate as electrolyte, supported by porous glass-paper disks. The required cathode pellets (7 mm in diameter) were prepared by pressing 20–30 mg of $In_{16}Fe_8S_{32}$ at ca. 3.5 tons. Cells were assembled under an argon atmosphere in a M-Braum glovebox. The water content inside the box was monitored with a humidity sensor and turned out to be 2–3 ppm H_2O.

Galvanostatic intermittent titration technique (GITT) and step potential electrochemical spectroscopy (SPES) were carried out by using the multichannel microprocessor-controlled system MacPile. Initial relaxation of the cell was allowed until the condition $\Delta V/\Delta t < 1$ mV/h was fulfilled.

[1] To whom correspondence should be addressed.

0022-4596/98 $25.00

For the GITT curve, the current intensity during the discharge was 19 μA ($\sim 50\ \mu A/cm^2$) for a period of 10 h (~ 0.5 Li/mol), followed by a relaxation process until the voltage variation was lower than 1 mV/h. For SPES curves, 10-mV potential steps were used. For each step, the voltage was kept constant for 2 h or until the current intensity during the relaxation process reached 1/10,000th of the initial current intensity. The lithiated samples were obtained by interrupting the galvanostatic discharge at the desired compositions. The average lithium composition of the cathodic material was calculated by Faraday's law by assuming that no current flow was due to side reactions.

X-ray powder diffraction patterns (XDPs) were recorded on a Philips diffractometer using Cu$K\alpha$ radiation. For the inserted samples, a plastic film was used to avoid the undesirable (oxidation) reactions with air during recording of the XDP. To study the structural modifications induced by the insertion reaction, Rietveld analysis of XDPs were carried out with the aid of the computer program Rietveld Analysis Program DBWS-9411 (9).

^{57}Fe Mössbauer spectra were recorded at room temperature in the constant-acceleration mode on an ELSCINT-AME40 spectrometer. The velocity scale was calibrated with the magnetic sextet spectrum of a high-purity iron foil absorber. The source was ^{57}Co(Rh). Recorded spectra were fitted to Lorentzian profiles by a least-squares method (10) and the fit quality was controlled by the classical χ^2 and misfit test.

X-ray absorption measurements were recorded using the synchrotron radiation of DCI storage ring at LURE (Orsay, France) in transmission mode. The apparatus was equipped with a Si (111) two-crystal monochromator. The samples were finely ground and passed through a 5-μm sieve to obtain a powder homogeneous in particle size. The powder was then dispersed in cyclo-hexane and deposed on a micropore membrane.

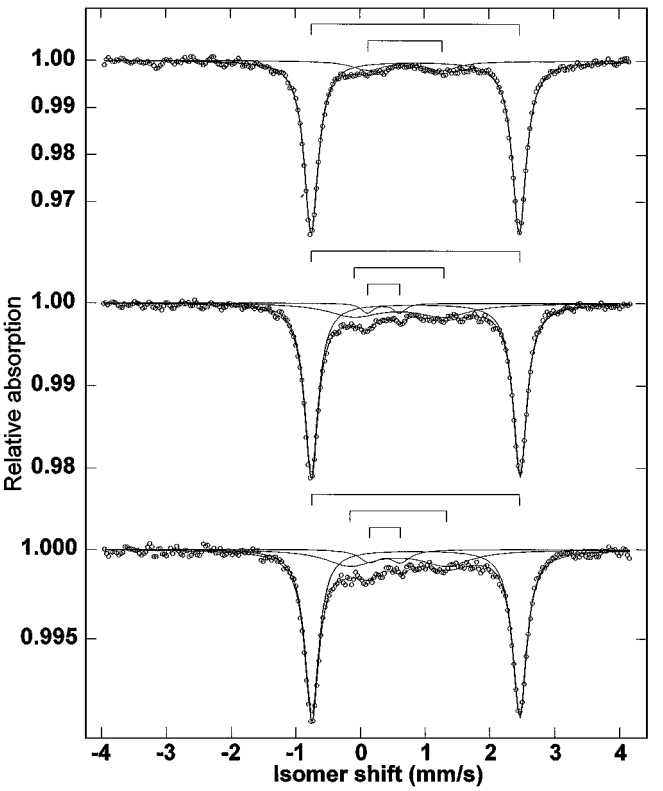

FIG. 1. Mössbauer spectra of $Li_xIn_{16}Fe_8S_{32}$ at $x = 2$ (top), $x = 8$ (middle), and $x = 14$ (bottom).

RESULTS AND DISCUSSION

Structural Analysis

To follow the structural modifications that take place during lithium insertion, XDPs and Mössbauer spectra were recorded at different lithium contents. The pristine compound is well known and has been characterized. The Mössbauer spectrum shows two doublets, corresponding to iron atoms in tetrahedral 8*a* and octahedral 16*d* sites. X-ray diffraction results are typical of a single phase and indexed in a spinel-related cubic system.

The Mössbauer spectra of some selected lithiated products are shown in Fig. 1. The results of the fitting for all the lithiated samples are listed in Table 1. The doublets with a quadrupole splitting QS = 3.22 and 1.1–1.5 mm/s are ascribable to iron atoms in octahedral 16*d* and tetrahedral 8*a* sites, respectively. For $x < 8$, a cation migration of Fe is observed from the 16*d* site (the relative area decrease) toward the 8*a* site (the relative area increases). At $x = 8$ another site appears (see Fig. 1). Comparison of the isomer shift with the chemically lithiated product allows us to ascribe it to a tetrahedral 8*b* site (8). It is worth noting that at 8 Li/mol, the 8*a* site is full and the 16*c* site has an occupancy factor of 0.5 (assuming that Li are placed in 16*c*). So, a new cation distribution appears in order to minimize the repulsion (as discussed above). For $x > 8$, the cation migrations go on from the octahedral site to the tetrahedral 8*a* and 8*b* sites. An additional effect is the increase in the quadrupole splitting and line width of the subspectra of the ^{57}Fe in tetrahedral coordination, indicating that distortion increases and charge distribution symmetry decreases during the insertion process. These phenomena can be explained by the presence of vacancies surrounding the tetrahedrally coordinated Fe atoms (11, 12).

Concerning the isomer shifts, there is no variation of the observed value for Fe atoms in the octahedral site 16*d*. On the other hand, in the range $0 < x \leq 8$, a slight decrease is obtained for the 8*a* site. Additionally, the isomer shift of the third occupied site (8*b*) is lower than for the other tetrahedral one (8*a*). These two facts reveal that an increase in covalency takes place during lithium insertion,

TABLE 1
Hyperfine Parameters of Mössbauer Spectra of $Li_xIn_{16}Fe_8S_{32}$: Isomer Shift (IS), Quadrupole Splitting (QS), Full Width at Half-Maximum (LW), and Relative Area (RA)

Site	x	IS (mm/s)	QS (mm/s)	LW (mm/s)	RA (%)
16*d* (O_h)	2	0.861(1)	3.2(1)	0.260(8)	89(2)
	4	0.861(1)	3.2(1)	0.252(8)	86(1)
	6	0.866(2)	3.2(1)	0.259(8)	83(1)
	8	0.864(1)	3.2(1)	0.254(8)	79(3)
	10	0.866(1)	3.2(1)	0.254(8)	74(2)
	12	0.860(1)	3.2(1)	0.259(9)	73(2)
	14	0.860(2)	3.2(1)	0.263(9)	69(4)
8*a* (T_d)	2	0.70(3)	1.15(5)	0.60(6)	11(2)
	4	0.67(3)	1.09(6)	0.80(8)	14(1)
	6	0.65(2)	1.08(4)	0.73(5)	17(1)
	8	0.57(4)	1.10(7)	1.0(1)	17(3)
	10	0.61(4)	1.39(7)	0.99(9)	22(2)
	12	0.61(4)	1.43(8)	1.2(1)	23(2)
	14	0.60(4)	1.50(8)	0.9(1)	24(2)
8*b* (T_d)	2	—	—	—	—
	4	—	—	—	—
	6	—	—	—	—
	8	0.11(4)	0.35(5)	0.3(1)	4(3)
	10	0.37(2)	0.50(3)	0.23(4)	4(2)
	12	0.28(3)	0.64(5)	0.35(3)	4(2)
	14	0.39(3)	0.48(4)	0.37(7)	7(4)

without reduction of Fe^{2+}. Similar behavior has been observed chemical lithium insertion (8).

Figure 2 shows the X-ray absorption spectra at L_I edge of In. In L_I absorption line suffers no changes on lithium insertion (4244.2 and 4244.3 eV for the pristine compound and $Li_{5.2}In_{16}Fe_8S_{32}$, respectively), thus indicating the absence of a clear reduction of In^{3+}. This fact, together with the Mössbauer results showing no reduction of Fe^{2+}, seems to indicate that the incoming electrons during the insertion process do not cause a net reduction of cations but an increase in covalency of the network (as deduced from ^{57}Fe Mössbauer spectroscopy), the electrons being incorporated into the delocalized band structure.

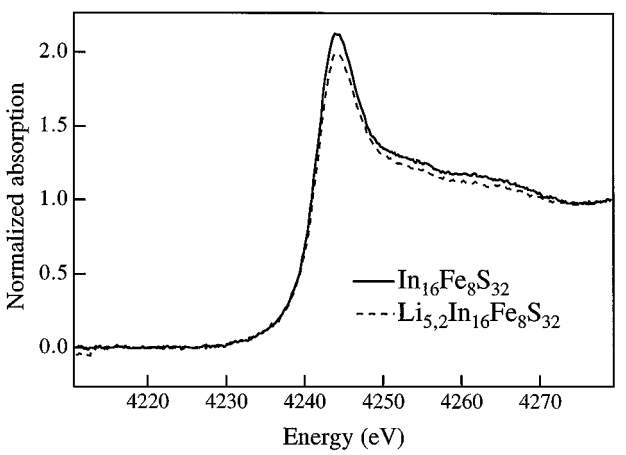

FIG. 2. X-ray absorption spectra at L_I–In edge of pristine $In_{16}Fe_8S_{32}$ (solid line) and lithiated $Li_{5.2}In_{16}Fe_8S_{32}$ (dotted line).

For a detailed structural analysis, Rietveld fitting of XDPs was carried out. The XDPs were characteristic of a single phase for all the lithiated samples. The procedure for the refinement makes use of the computer program developed by Wiles and Young (9), as described under Experimental. Figure 3 shows the results for some selected samples. A line broadening of the diffraction peaks was observed, reflecting an amorphization process during lithium insertion. The cell parameters and the cation distributions obtained by Rietveld refinement are listed in Table 2. At low lithium contents, a migration of Fe atoms from 16*d* to 8*a* is observed, in agreement with the Mössbauer data, whereas In atoms move from 8*a* to 16*d*. At $x = 6$, the 16*c* site is also occupied by In, but the occupancy factor is only 0.2. At $x = 8$, the migration goes on, the amount of In in 16*c* increases, and a new site is occupied by Fe atoms. This new site (8*b*) is also observed in Mössbauer spectra. At higher lithium contents In atoms leave the 16*c* site and the migration from 8*a* toward 16*d* is always observed. With respect to Fe atoms, the situation does not change. Only for $x = 14$ is a slight additional migration from 16*d* to 8*a* observed. These results are in good agreement with the analysis of the Mössbauer spectra. Finally, Fig. 4 shows the evolution occupancy factors obtained by X-ray diffraction and Mössbauer spectroscopy for its comparison. On the other hand, the cell parameters remain almost constant during the insertion. So, the general trend for accommodating the inserted atoms is not an expansion but a cation redistribution, characterized by a migration of In from 8*a* to 16*d*, while Fe moves from 16*d* to 8*a*.

Electrochemical Behavior

Figure 5 shows the continuous galvanostatic discharge and GITT curves. Both are characterized by a region of nearly constant voltage or apparent plateau form $x \approx 0$ to ca. 7 Li/mol. For higher lithium contents, the slope of the discharge curve increases (in negative value). This fact is less evident for the GITT curve.

The occurrence of the plateau in the voltage–composition curve is analyzed by using the classification of insertion electrodes proposed by Armand (13). It includes three different insertion models that may lead to flat regions in the V–x curves by multiphase or pseudomultiphase mechanisms:

a. Lattice relaxation pressure, when two phases are present. From XDP we conclude that only one phase is present

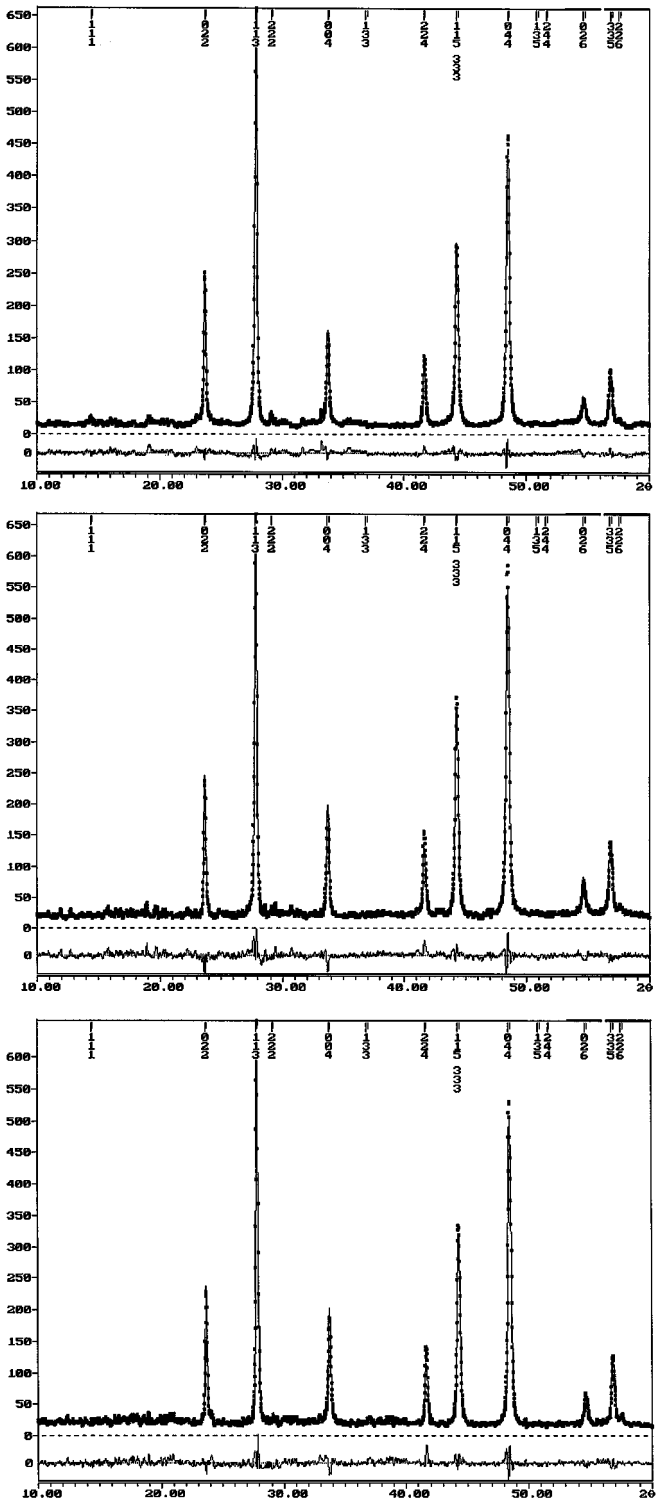

FIG. 3. XDP and Rietveld refinement of $Li_xIn_{16}Fe_8S_{32}$ at $x = 2$ (top), $x = 8$ (middle), and $x = 14$ (bottom).

in the first composition domain (up to ca. 7 Li/mol). On the other hand, for high lithium contents, the possible presence of a second amorphous phase cannot be neglected.

TABLE 2
Results of the Rietveld Analysis of X-Ray Diffraction Data of $Li_xIn_{16}Fe_8S_{32}$, According to the Space Group $Fd\bar{3}m$ (Origin at $\bar{3}m$)

		Fe			In			
x	a (Å)	8*a*	8*b*	16*d*	8*a*	16*c*	16*d*	R_{Bragg}
2	10.6080(5)	0.5(2)	—	7.5(2)	7.5(1)	—	8.5(1)	5.42
4	10.6093(7)	0.8(1)	—	7.2(1)	7.2(1)	—	8.8(1)	5.29
6	10.6119(5)	1.1(1)	—	6.9(1)	6.9(1)	0.2(1)	8.9(1)	4.92
8	10.6114(5)	1.5(1)	0.4(1)	6.1(1)	6.4(1)	0.3(1)	9.3(1)	4.50
10	10.6074(7)	1.5(1)	0.5(1)	6.0(1)	6.2(1)	0.2(1)	9.6(1)	4.90
12	10.6062(4)	1.54(5)	0.46(5)	6.00(5)	6.36(5)	0.12(5)	9.52(5)	4.52
14	10.6118(5)	1.70(5)	0.43(5)	5.87(5)	6.30(5)	—	9.70(5)	4.78

b. The intercalation pressure, which implies the ordering of the intercalated cations and the formation of stages in the case of layered materials. No changes in crystal symmetry or unit cell dimensions that could be interpreted in terms of ordered superstructures were detected, as shown by the XDPs.

c. Adjacent domains, where ordered phases can appear as the concentration of the inserted cation increases. These phases have their origin in the existence of more than one set of nonequivalent sites available, due to different geometries or repulsions between adjacent ions. Although the saturation of each phase is obtained only at total lattice saturation, if these domains are clearly different, they can be treated independently. The fact that different sites with different geometry (tetrahedral and octahedral) are available for lithium insertion into the spinel structure makes possible a mechanism based in this model to account for the shape of the GITT curve.

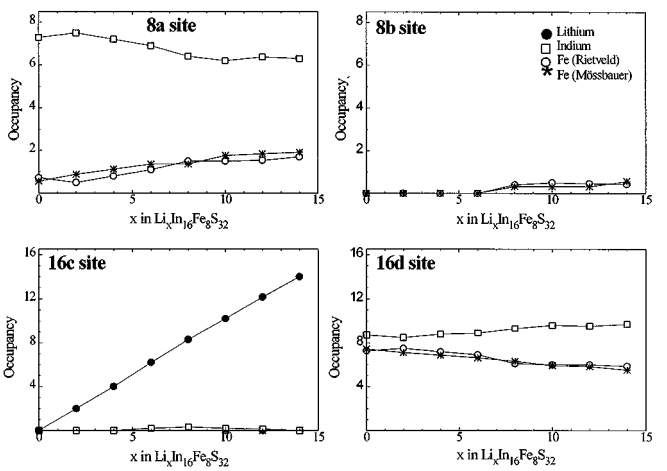

FIG. 4. Evolution of the occupancy of 8*a*, 8*b*, 16*c*, and 16*d* sites as a function of lithium content.

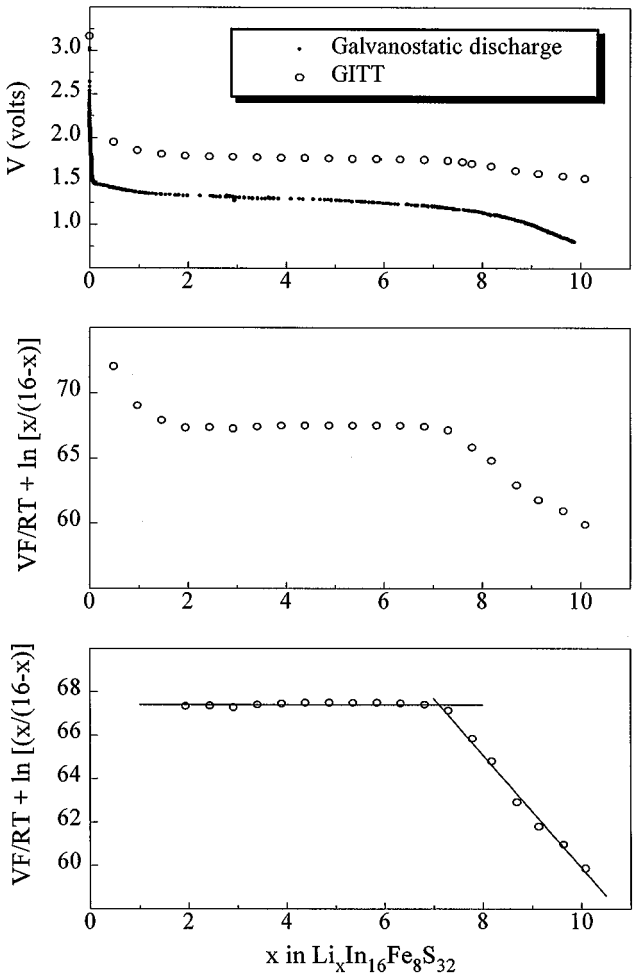

FIG. 5. Top: galvanostatic discharge and GITT of $In_{16}Fe_8S_{32}$ as cathode material. Middle: result of the application of Eq. [2] (Armand's model) to GITT data. Bottom: result of the application of Eq. [2]. The two insertion processes have been treated independently.

As model c implies a multidomain single-phase mechanism, the variation of the voltage as a function of the composition can be approximated to a mathematical expression similar to that corresponding to perfectly nonstoichiometric compounds, which is given by

$$V = E^0 - \frac{RT}{F} \ln \frac{x}{1-x} - \frac{RT}{F} g\left(x - \frac{1}{2}\right), \qquad [1]$$

where R is the gas constant, T the temperature, F Faraday's constant, E^0 the emf of the cell at standard conditions at $x = 1/2$, and g a temperature-dependent factor that takes into account the electrostatic repulsion between the inserted atoms. It can be positive or negative for repulsive or attractive interactions, respectively. Rewriting this equation,

$$V \frac{F}{RT} + \ln \frac{x}{1-x} = E^0 \frac{F}{RT} + \frac{g}{2} - gx, \qquad [2]$$

which represents a straight line as a function of x whose slope is g. Figure 5 shows the result of the application of Eq. [2] to GITT data. Two composition domains are now well defined: for $x = 2$ to 7 Li/mol and for $x > 7$. Treating both regions separately and fitting to Eq. [2], we obtain characteristic values of g and E^0 for each of the two domains of composition. For the first domain, the values are $E^0 = 1.741$ V and $g = 0.0018$. This means that the voltage of the first plateau is ca. 1.74 V. The low value of g indicates that the interactions between inserted ions are almost negligible. For the second domain, the value of E^0 is 1.671 V and g is 2.60, indicating that now the interactions are repulsive. This fact is discussed below, on the basis of the results of lithium diffusivity and thermodynamic factors. On the other hand, the electrochemical data in Fig. 5 do not fit the proposed model well in the range $0 < x < 2$. Several effects can be responsible for the observed discrepancy. In particular, a nonhomogeneous distribution of lithium within and between the chalcogenide particles could make useless the model on which Eq. [2] is based during the first steps of insertion (up to 0.06 Li per S).

In Fig. 6 the results of the SPES technique are shown. The presence of the two domains is not well resolved and only a plateau is clearly observed, which is centered at ca. 1 V. This fact is more evident in the incremental capacity curves and may be a consequence of being more apart from the strict equilibrium conditions than in GITT data. Additionally, the total amount of lithium obtained from SPES measurements is greater than that obtained from GITT experiments when the reduction process duration is shorter. This apparent discrepancy between GITT and SPES data is a result of the different conditions used in each study. Thus, the shorter duration of the reduction process in SPES experiment leads to a poorer resolution of the different processes. In this way, the region corresponding to a true insertion process overlaps with the plateau corresponding to the amorphization process and results in a curve that extends more than 15 F/mol.

Two effects are worth noting in the SPES data obtained during cell charge: first, a moderate polarization, as the plateau of the charge curve is centered at ca. 1.7–1.8 V; second, a good reversibility for insertion contents higher than 7–8 Li/mol. For charges recorded after insertion of lower lithium contents, a rapid increase in voltage took place before the extraction of lithium was complete. This fact is in good agreement with the GITT results. A repulsive interaction between the inserted ions can help its extraction during the charge. On the contrary, the absence of strong interionic repulsions found for $x < 7$ makes the extraction more difficult, and a strong increase in voltage during the charge is observed.

The chemical diffusion coefficient (D) was obtained from GITT and SPES measurements. The GITT method used was that reported by Honders *et al.* (14), based on the

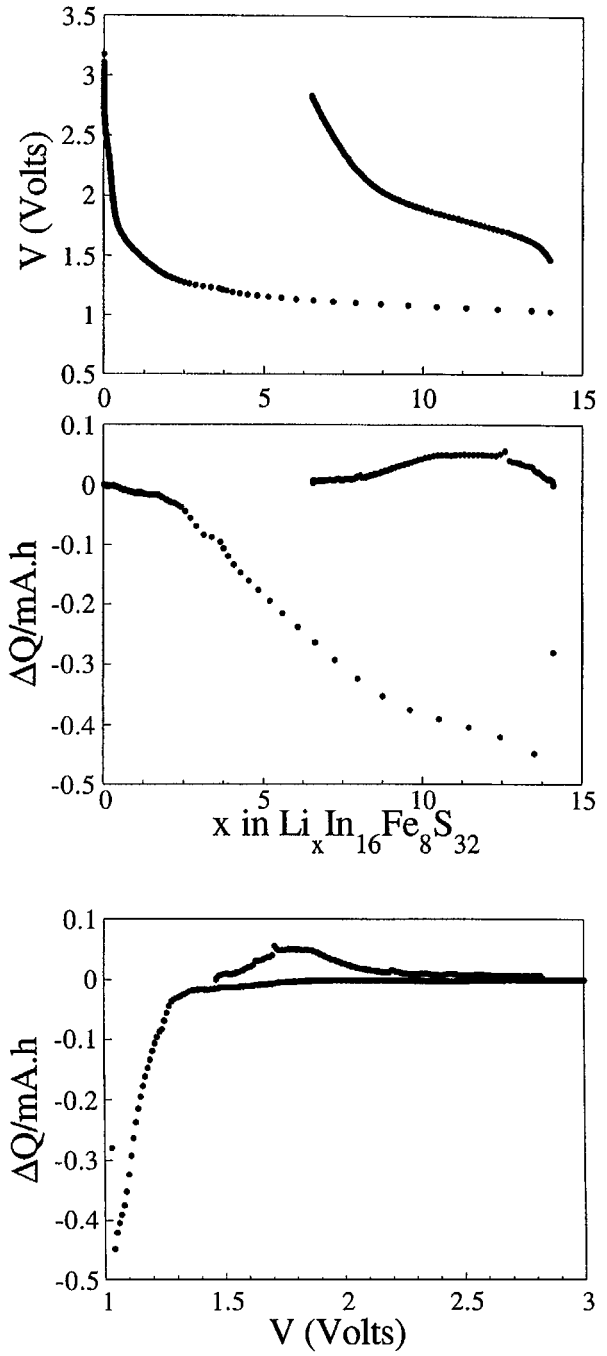

FIG. 6. Results of SPES of $In_{16}Fe_8S_{32}$: discharge curve (top) and incremental capacity as a function of lithium content (middle) and as a function of voltage (bottom).

analysis of the voltage evolution during the relaxation. The diffusion coefficient of lithium ions may also be deduced from SPES measurements by using the current–time relationship. At long times, the current decays exponentially to zero. When the condition $\tau > 0.25$ is fulfilled the current response function can be expressed as (14)

$$\ln i = \ln\left(\frac{\Delta E}{R + Z/3}\right) - \frac{DZ}{\delta^2(R + Z/3)}\, t, \qquad [3]$$

where $R = R_\Omega + R_{ct}$ (the ohmic resistance of the electrolyte and the electrodes and the charge transfer resistance of the interfaces, respectively) and ΔE is the step of the SPES. From the first term, $R + Z/3$ can be calculated, and from GITT measurements, the value of Z can also be estimated. Thus, from the slope of the plot $\ln i$ versus t, the value of D can also be obtained.

The values of D/δ^2 obtained are shown in Fig. 7. Data from SPES measurements also have an error in the values of x, as the insertion content varies during the relaxation process. For each experimental point, the error bar extends from the initial to the final value of x during the relaxation step. It is worth noting the similarity in the sequences obtained by both methods despite the difference in evaluation technique. The two sets of values are in good agreement. Both curves evidence the presence of two domains. The first one extends to $x \approx 7$ and is characterized by

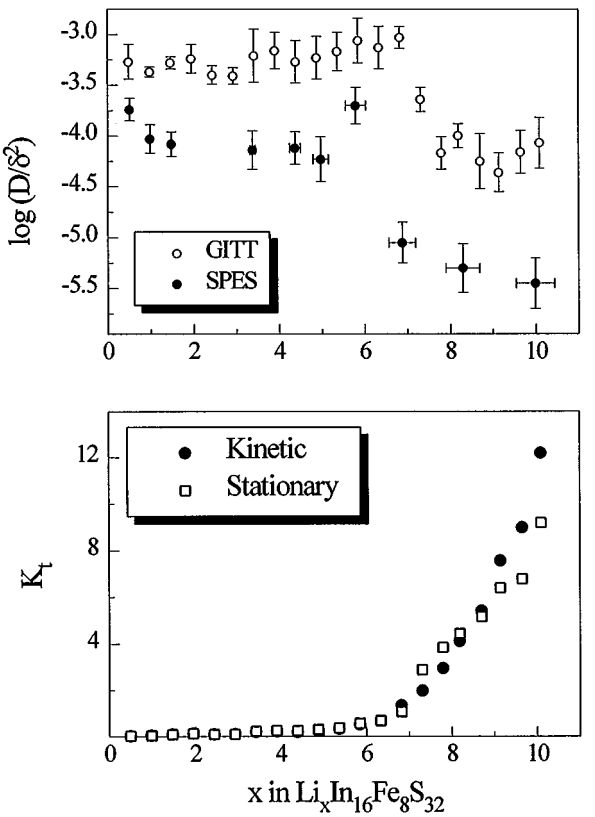

FIG. 7. Diffusion coefficient values obtained from GITT and SPES measurements (top) and K_t kinetic and stationary calculated from GITT measurements (bottom).

a relatively high value of D^2 ($\sim 1.3 \times 10^{-7}$ cm^2 s^{-1}). For $x > 7$, a second diffusion process appears with a lower value of D^2 ($\sim 1.5 \times 10^{-8}$ cm^2 s^{-1}). This behavior is similar to that observed for $Li_xIn_{16}Sn_4S_{32}$ (4), where two different diffusion processes are present (for $0 < x < 8$ and $x > 8$), with similar values of D. These values are also similar to those observed in some layered sulfides, such as Li_xTiS_2 (5×10^{-8} to 5×10^{-9} cm^{2}s^{-1}) and Li_xTaS_2 (1.5×10^{-8} cm^2 s^{-1}) (15, 16). The presence of these two diffusion processes is also in good agreement with the analysis of the GITT curve and the presence of two domains of discharge.

K_t can be calculated from kinetic measurements from Honders and colleagues' model, but it can also be obtained from stationary measurements (14). In this case,

$$K_t = -\frac{xF}{RT}\frac{\Delta V}{\Delta x}. \qquad [4]$$

By determining the slope of the GITT curve at different stoichiometries, the thermodynamic factor may be obtained as a function of the degree of insertion (x). From Fig. 7 one can see that the two sets of values are consistent, which is indirect proof of the reliability of the applied method. For $x > 7$, K_t strongly increases. The effect on K_t and the change in the value of the diffusion coefficient can be attributed to significant structural modifications undergone by the host on insertion and to the strong electrostatic repulsions between inserted ions. These results confirm the values of g according to Armand's model, where for $x > 7$ a repulsive interaction between inserted lithium ions has been deduced and is in good agreement with the structural analysis, which shows that for $x > 7$ all typical available sites (8*a*, 8*b*, 16*c*, 16*d*) are partially occupied. It is worth noting that, in some spinel systems, a transition to rock-salt structure has been described during the insertion process (17). This transition is characterized by an insertion of Li ions in the 16*c* site and a migration of A cations from the 8*a* to the 16*c* site. Finally, this process may yield compounds with empty T_d sites and all O_h sites filled with metal ions. In iron, indium spinel sulfide, a limit situation is obtained for $x = 8$. For higher lithium contents, both 8*a* and 16*c* (or 8*b* and 16*d*) sites tend to be occupied. Since these sites are close to each other (8*a* to 16*c* and 8*b* to 16*d*), an increase in electrostatic repulsions is expected. Other different cation distributions are possible, as we have recently shown (8), by occupying simultaneously 8*a*, 8*b*, 16*c*, and 16*d* sites. In all cases, the cations can be redistributed to minimize the repulsive interactions up to 8 Li/mol. For contents higher than 8, direct interactions between cations are present. This fact confirms the observed evolution of K_t as a function of the degree of insertion x.

[2] These values have been obtained using as diffusion path (δ) the thickness of the pellet used as cathode in the lithium cell.

CONCLUSION

During electrochemical lithium insertion into $In_{16}Fe_8S_{32}$, there are two different steps. For $x < 7$, a pseudo-plateau at ca. 1.74 V has been identified in the discharge curve. The analysis according to the Armand's model gives a negligible interaction between inserted ions. The Mössbauer spectra show two different environments of Fe atoms, with no reduction of Fe cations. Data from X-ray absorption spectroscopy also indicates that there is no reduction of In cations. Thus, the incoming electrons are incorporated into the delocalized band structure, increasing the covalency of the network. For $x > 7$, a second domain is present, centered at ca. 1.67 V. The value of g indicates the presence of weak but nonnegligible repulsive interactions between inserted ions, which is confirmed by a strong increase in K_t and by kinetic data as a decrease in the values of lithium diffusivity obtained by both GITT and SPES techniques. A third environment of Fe atoms appears in this composition region. The charge curve shows that this second domain, but not the first, is reversible. Additionally, during lithium insertion, a migration of In and Fe atoms is observed by both X-ray diffraction and Mössbauer spectroscopy. The main structural effect of insertion consists of a migration of In cations from the 8*a* site toward 16*d* site, while Fe atoms move from the 16*d* site to the 8*a* site, without marked changes in unit cell dimensions. In addition, the insertion process increases the bond covalency, without a clear reduction in neither Fe^{2+} or In^{3+}.

ACKNOWLEDGMENTS

The authors are indebted to the European Community and the Ministries of Foreign Office (France) and Education (Spain) for financial support (Contract JOU2-CT93-026, Human Capital and Mobility No. ERBCHBGCT 93.0430, Training and Mobility of Researchers No. ERBFMBICT 96.0768, and PICASSO Program).

REFERENCES

1. M. Eisenberg, *J. Electrochem. Soc.* **127,** 2382 (1980).
2. A. C. W. P. James, B. Ellis, and J. B. Goodenough, *Solid State Ionics* **27,** 45 (1988).
3. M. Pernet, P. Strobel, B. Bonnet, and P. Bordet, *Solid State Ionics* **66,** 259 (1993).
4. J. Morales, J. L. Tirado, M. L. Elidrissi Moubtassim, J. Olivier-Fourcade, and J. C. Jumas, *J. Alloys Compds.* **217,** 176 (1995).
5. M. A. Cochez, J. C. Jumas, P. Lavela, J. Morales, J. Olivier-Fourcade, and J. L. Tirado, *J. Power Sources*, **62,** 99 (1996).
6. M. L. Elidrissi Moubtassim, J. Olivier-Fourcade, J. Senegas, and J. C. Jumas, *Mater. Res. Bull.* **28,** 1083 (1993).
7. A. F. Wells, *in* "Structural Inorganic Chemistry," 4th ed., p. 491, Clarendon Press, Oxford, 1975.
8. C. Bousquet, A. Krämer, C. Pérez Vicente, J. L. Tirado, J. Olivier-Fourcade, and J. C. Jumas, *J. Solid State Chem.* **134,** 238 (1997).
9. D. B. Wiles and R. A. Young, *J. Appl. Cryst.* **28,** 366 (1995).
10. W. Kündig, *Nucl. Instrum. Methods* **75,** 336 (1969).

11. M. Womes, J. Olivier-Fourcade, J. C. Jumas, F. Aubertin, and U. Gonser, *J. Solid State Chem.* **97,** 249 (1992).
12. M. Womes, F. Py, M. L. Elidrissi Moubtassium, J. C. Jumas, J. Olivier-Fourcade, F. Aubertin, and U. Gonser, *J. Phys. Chem. Solids* **55,** 1323 (1994).
13. M. Armand, *in* "Materials for Advanced Batteries" (D. W. Murphy, J. Broadhead, and B. C. H. Steele, Eds.), p. 145, Plenum, New York, 1980.
14. A. Honders, J. M. der Kinderen, A. H. van Heeren, J. H. W. Wit, and G. H. J. Broers, *Solid State Ionics* **15,** 265 (1985).
15. S. Basu and W. L. Worrell, *in* "Fast Ion Transport in Solids" (P. Vashitsha, J. N. Mundy, and G. K. Shenoy, Eds.), p. 149, North-Holland, Amsterdam, 1979.
16. A. S. Nagelberg and W. L. Worrell, *in* "Symposium on Electrode Materials and Processes for Energy Conversion and Storage" (J. D. E. McIntire, S. Srinivasan, and F. G. Will, Eds.), p. 84, Electrochem. Soc., Princeton, 1977.
17. M. M. Thackeray, W. I. F. David, and J. B. Goodenough, *Mater. Res. Bull.* **17,** 785 (1982).